ACS APPLIED MATERIALS & INTERFACES

Research Article

www.acsami.org

Strong Piezoelectricity in (1 − x)($K_{0.4}Na_{0.6}$)($Nb_{0.96}Sb_{0.04}$)O_3-$xBi_{0.5}K_{0.5}Zr_{1-y}Sn_yO_3$ Lead-Free Binary System: Identification and Role of Multiphase Coexistence

Ting Zheng, Jiagang Wu,* Dingquan Xiao, and Jianguo Zhu

Department of Materials Science, Sichuan University, Chengdu 610064, P. R.China

Xiangjian Wang, Lipeng Xin, and Xiaojie Lou

Multi-disciplinary Materials Research Center, Frontier Institute of Science and Technology, and State Key Laboratory for Mechanical Behavior of Materials, Xi'an Jiaotong University, Xi'an 710049, P. R. China

Supporting Information

ABSTRACT: Here we report a strong piezoelectric activity in (1 − x)($K_{0.4}Na_{0.6}$)($Nb_{0.96}Sb_{0.04}$)O_3-$xBi_{0.5}K_{0.5}Zr_{1-y}Sn_yO_3$ lead-free ceramics by designing different phase boundaries. The phase boundaries concerning rhombohedral-orthorhombic-tetragonal (R-O-T) and rhombohedral-tetragonal (R-T) multiphase coexistence were attained by changing BKZS and Sn contents and then were identified by the X-ray diffraction patterns as well as temperature-dependent permittivity and $\nu 1$ Raman modes associated with BO_6 perovskite octahedron. A high strain (strain = 0.21−0.28% and d_{33}* = 707−880 pm/V) and a strong piezoelectric coefficient (d_{33} = 415−460 pC/N) were shown in the ceramics located at the multiphase coexistence region. The reported results of this work are superior to that (d_{33}* ∼ 570 pm/V and d_{33} ∼ 416 pC/N) of the textured (K,Na,Li)(Nb,Ta,Sb)O_3 ceramics [*Nature* **2004**, *432*, 84]. We believe that the material system of this work will become one of the most promising candidates for piezoelectric actuators.

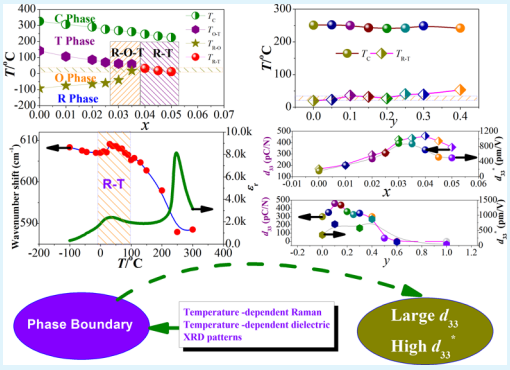

KEYWORDS: *potassium−sodium niobate, multiphase coexistence, strong piezoelectric activity, physical mechanism*

INTRODUCTION

Lead-based ceramics possess an excellent piezoelectric constant (d_{33}) and high electric field-induced strain[1] and are currently applied in many electronic devices. However, most researchers have recently given considerable attention to lead-free piezoceramics because the hazardous Pb element will be gradually prohibited in electronic devices.[2−40] Due to the importance of high strain in piezoelectric actuators, related research has recently become very active.[2−14,30−35] Previously, it was reported that a high strain could be well developed in the $Bi_{1/2}Na_{1/2}TiO_3$ (BNT)-based ceramics,[2−4] but the poor d_{33} values (<200 pC/N) as well as high driving electric fields inevitably hinder their practical applications.[2−4] For example, a large strain of 0.45% under a high driving electric field (∼8 kV/mm) was achieved in ($Bi_{0.5}Na_{0.5}$)TiO_3−$BaTiO_3$-(K,Na)NbO_3, and unfortunately there is a poor d_{33} (<100 pC/N).[2] Although enhanced d_{33} and d_{33}* can be simultaneously observed in $BaTiO_3$-based ceramics, a very low T_C was always shown.[5−9] As a result, there are some incongruous developments between piezoelectricity and strain in the field of lead-free piezoelectrics.

In 2004, textured (K,Na,Li)(Nb,Ta,Sb)O_3 ceramics were shown to exhibit an enhanced d_{33} of ∼416 pC/N and a high converse piezoelectric coefficient (d_{33}* = S_{max}/E_{max} ∼ 750 pm/V).[10] Since then, (K,Na)NbO_3 (KNN) ceramics have been considered as promising candidates to replace the lead-based ones.[11−19] Nevertheless, a relatively low strain (0.1−0.2%) was observed in KNN-based ceramics prepared by conventional solid-state methods.[11−14] Therefore, it has become an urgent task to search for a kind of KNN-based ceramics with balanced developments of d_{33} and d_{33}*.

In the past several years, there have been some reports on the strain investigations in ($Bi_{0.5}Na_{0.5}$)TiO_3 and $BaTiO_3$-based ceramics, and the Sn^{4+} substitutions for Ti^{4+} site can effectively enhance their strain behavior.[2−9] For example, a relatively high d_{33}* value of 585 pm/V can be observed when the 5% mol SnO_2 was used to modify $Bi_{0.5}(Na_{0.82}K_{0.18})_{0.5}TiO_3$.[4] Furthermore, the Sn can promote piezoelectric and strain behavior of $BaTiO_3$-based ceramics.[5] As a result, it was highly expected that the doping with Sn^{4+} may improve the strain behavior of KNN-based ceramics. To our knowledge, there were few reports on the strain investigations on the Sn-doped KNN ceramics together with a strong piezoelectric activity. In addition, the

Received: January 7, 2015
Accepted: February 20, 2015
Published: March 3, 2015

DOI: 10.1021/acsami.5b00151
ACS Appl. Mater. Interfaces 2015, 7, 5927−5937

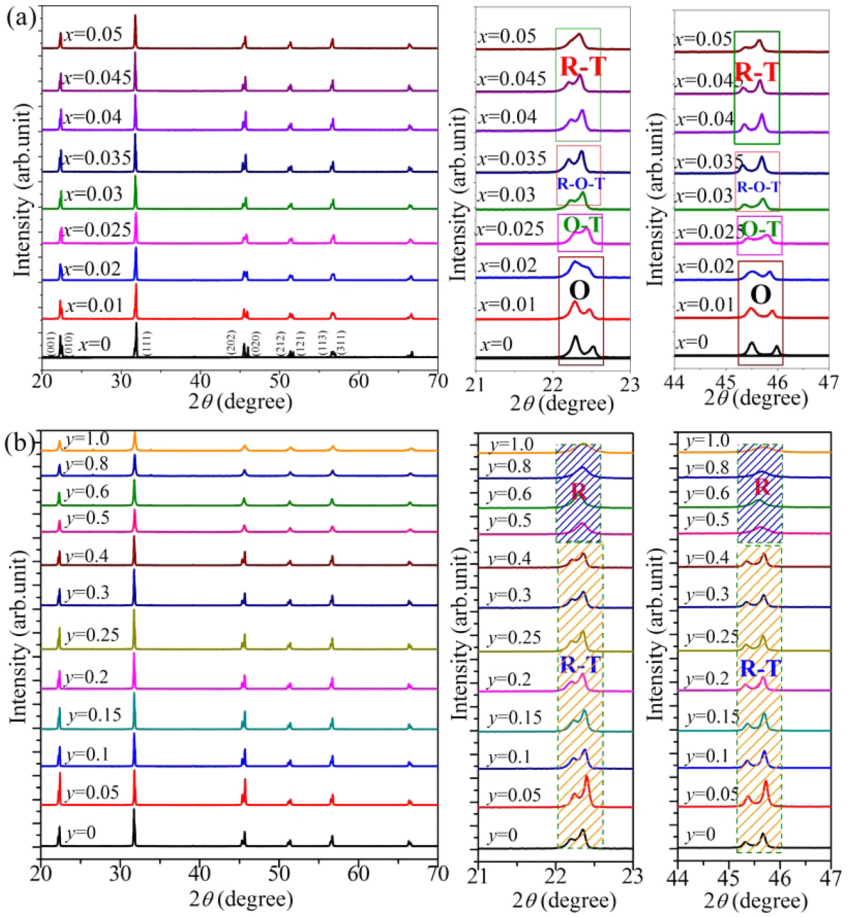

Figure 1. XRD patterns of $(1-x)(K_{0.4}Na_{0.6})(Nb_{0.96}Sb_{0.04})O_3$-$xBi_{0.5}K_{0.5}Zr_{1-y}Sn_yO_3$ ceramics with (a) $0 \le x \le 0.05$, $y = 0.1$, (b) $x = 0.04$, $0 \le y \le 1.0$.

rhombohedral-tetragonal (R-T) multiphase coexistence of KNN-based ceramics is usually evaluated by the temperature-dependent dielectric constant.[15−17] It is often suspected that an intermediate phase may exist in the mixed phases, which bridges the T and R phases. To clarify this suspension, some tools should be used to further confirm the phase boundaries. In this work, we identified the phase compositions of R-T phase boundary in KNN-based ceramics by considering their corresponding temperature dependence of the Raman spectrum.

In this work, a new $(1-x)(K_{0.4}Na_{0.6})(Nb_{0.96}Sb_{0.04})O_3$-$xBi_{0.5}K_{0.5}Zr_{1-y}Sn_yO_3$ ceramic system has been fabricated via normal sintering, and the Sn is particularly used to modify electrical properties by tailoring the phase boundaries. The different phase boundary types (e.g., O-T, R-O-T, and R-T) were tuned by changing BKZS and Sn contents. In addition, the objective of this work is clearly addressed: (i) Constructing multiphase coexistence by the composition design; (ii) identify the existence of R-T phase boundary and obtain large d_{33} as well as high d_{33}*; (iii) investigate the relationships between phase boundaries and piezoelectricity. In this work, the addition of BKZS and Sb^{5+}, respectively, induces the formation of R-O-T and R-T phase boundaries in the composition range of $0.03 \le x \le 0.035$ and $0.04 \le x \le 0.05$. Sn^{4+} is applied to improve strain behavior, accompanied by the formation of R-T phase boundary for $0 \le y \le 0.4$. A high d_{33}* of ∼880 pm/V and a large d_{33} of ∼460 pC/N were observed in the ceramics with $x = 0.03$, $y = 0.1$ and $x = 0.04$, $y = 0.1$, respectively. As a result, a large d_{33}* and a high d_{33} could be attained in Sn-doped KNN ceramics by tuning its composition, demonstrating that the material system is one of the most promising candidates for actuator applications.

EXPERIMENTAL SECTION

Ceramics with a formula $(1-x)(K_{0.4}Na_{0.6})(Nb_{0.96}Sb_{0.04})O_3$-$xBi_{0.5}K_{0.5}Zr_{1-y}Sn_yO_3$ were synthesized by the conventional solid-state sintering method, and raw materials {e.g. K_2CO_3 (99%), Na_2CO_3 (99.8%), Nb_2O_5 (99.5%), Sb_2O_3 (99.99%), Bi_2O_3 (99.999%), SnO_2 (99.8%), and ZrO_2 (99%)} were weighed with an electronic balance and then were ball milled for 24 h with alcohol. These dried powders were calcined at 850 °C for 6 h and then were mixed with a binder of 8 wt % poly(vinyl alcohol) (PVA). These calcined powders were pressed into disks with a diameter of 10 mm and a thickness of 1 mm under a pressure of 10 MPa. After PVA was burned off, the pellets were sintered at 1085−1095 °C for 3 h in air. The sintered samples were pasted with silver and then fired at 600 °C for 10 min. Finally, a direct current electric field of 2−4 kV/mm was applied to pole each sample in a silicon oil bath at 30 °C.

X-ray diffraction (XRD) (Bruker D8 Advanced XRD, Bruker AXS Inc., Madison, WI, Cu Kα) in the $\theta-2\theta$ scanning mode and a step of 0.02° was used to characterize the crystal structures of the ceramics. HR LabRam Raman spectroscopy system was used to measure the temperature (−100−300 °C) dependence of the Raman spectrum, where a 514 nm Ar laser was used for excitation. Field emission-scanning electron microscopy (FE-SEM) (JSM-7500, Japan) was used to characterize the surface microstructure and the element mapping. The curves of the dielectric constant against temperatures (ε_r-T) were tested by a programmable furnace in connection with an LCR analyses (HP 4980, Agilent, Santa Clara, CA). The dielectric properties of each poled sample were measured by an impedance analyzer (HP 4294A).

DOI: 10.1021/acsami.5b00151
ACS Appl. Mater. Interfaces 2015, 7, 5927−5937

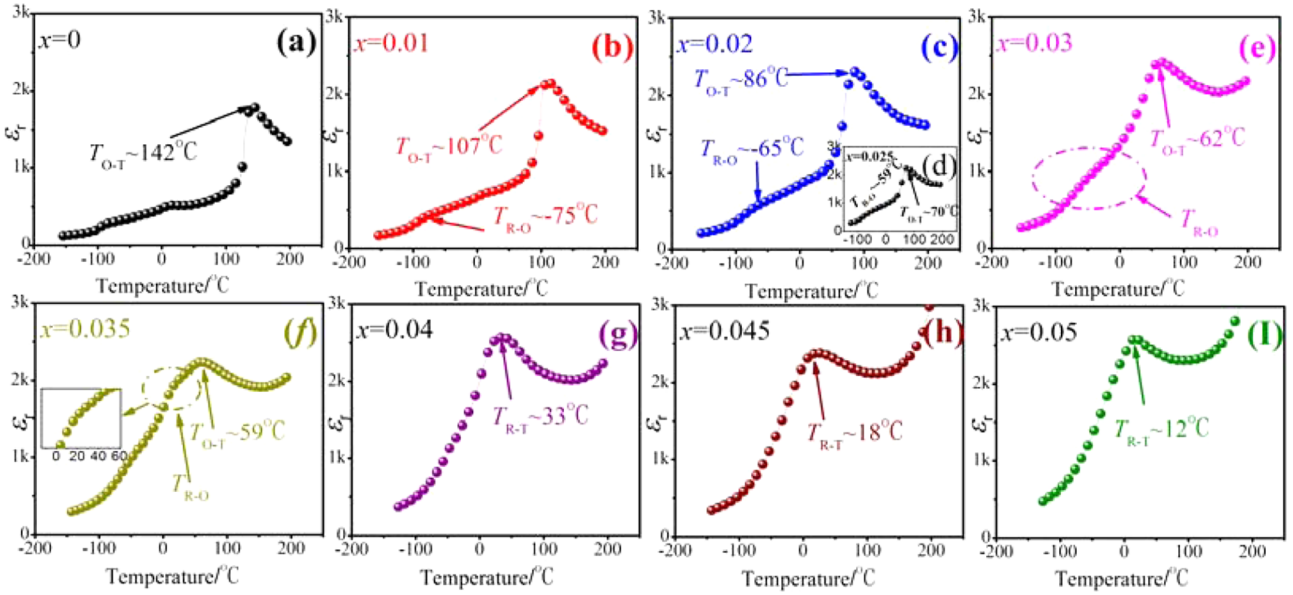

Figure 2. ε_r–T (−150–200 °C) curves of the ceramics with different x contents: (a) x = 0, (b) x = 0.01, (c) x = 0.02, (d) x = 0.025, (e) x = 0.03, (f) x = 0.035, (g) x = 0.04, (h) x = 0.045, and (i) x = 0.05.

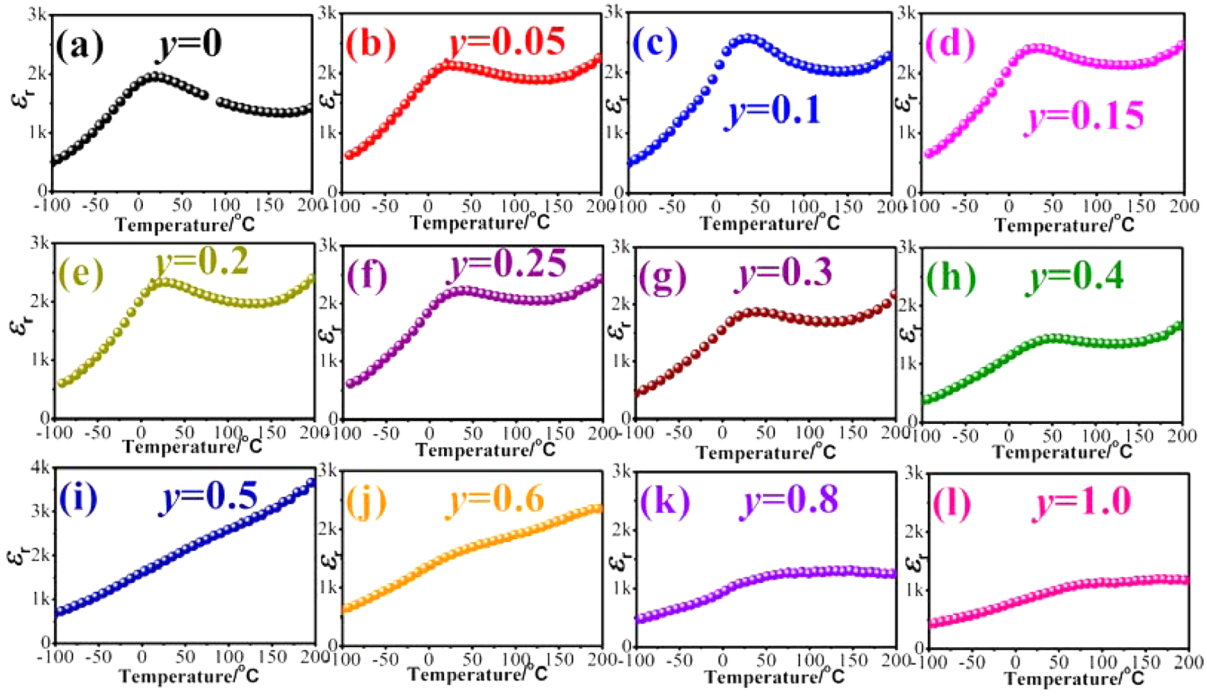

Figure 3. ε_r–T (−100–200 °C) curves of the ceramics with different y contents: (a) y = 0, (b) y = 0.05, (c) y = 0.1, (d) y = 0.15, (e) y = 0.2, (f) y = 0.25, (g) y = 0.3, (h) y = 0.4, (i) y = 0.5, (j) y = 0.6, (k) y = 0.8, and (l) y = 1.0.

A Radiant Precision Workstation (USA) was used to measure the P–E hysteresis loops with a frequency of 10 Hz. Furthermore, the piezoelectric constant d_{33} and the planar electromechanical coupling factor k_p were measured by a piezo-d_{33} meter (ZJ-3 A, China) and impedance analyzer (HP 4194A), respectively. At last, the electric field induced strain was measured.

RESULTS AND DISCUSSION

In this work, the phase evolutions of the $(K,Na)(Nb,Sb)O_3$-$(Bi,K)(Zr,Sn)O_3$ binary system were analyzed by characterizing both XRD patterns and ε_r–T curves, and particularly the R-T phase boundary was further confirmed by the temperature-dependent Raman spectrum. Figure 1a,b displays the room-temperature XRD patterns of $(1-x)(K_{0.4}Na_{0.6})(Nb_{0.96}Sb_{0.04})$-$O_3$-$xBi_{0.5}K_{0.5}Zr_{1-y}Sn_yO_3$ ceramics as a function of x and y, respectively. All ceramics exhibit a typical perovskite structure without secondary phases, suggesting that both KNNS and BKZS formed a stable solid solution. Figures 2 and 3, respectively, give the ε_r–T curves of the ceramics with different x and y contents, measured at −150–200 °C and 100 kHz. According to the results of both XRD and ε_r–T (see Figures 1–3), the phase evolutions of the ceramics were analyzed. One can see from Figure 1a that an orthorhombic (O) phase was shown in the $(1-x)(K_{0.4}Na_{0.6})(Nb_{0.96}Sb_{0.04})O_3$-

DOI: 10.1021/acsami.5b00151
ACS Appl. Mater. Interfaces 2015, 7, 5927–5937

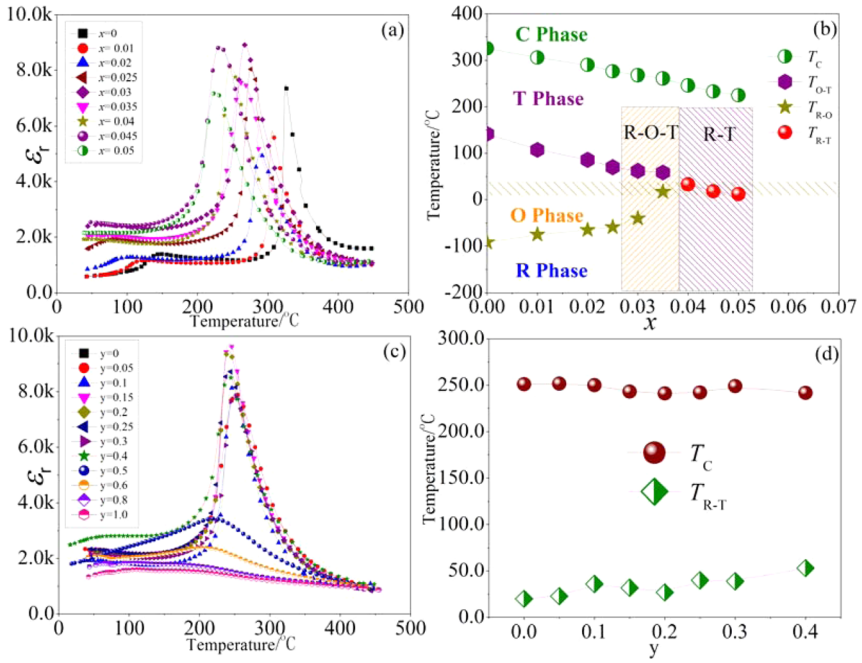

Figure 4. (a and c) ε_r–T (30–450 °C) curves of the ceramics with different x and y, respectively. (b and d) Phase diagrams of the ceramics with different x and y, respectively.

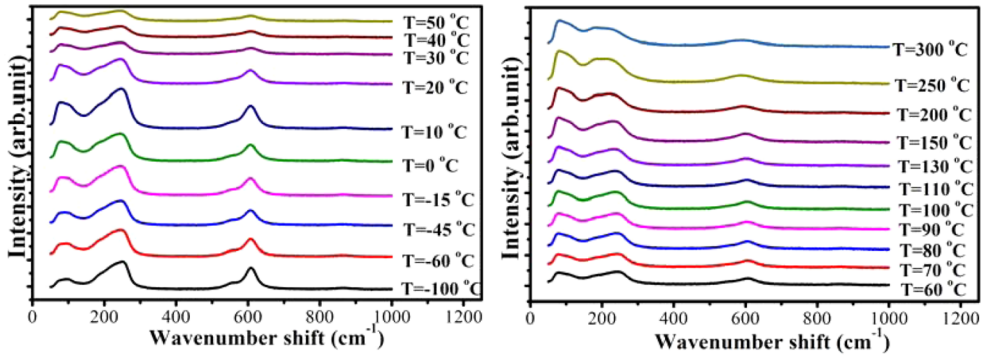

Figure 5. Raman spectra in the wavenumber ranges from 50 to 1000 cm^{-1} of the ceramic with x = 0.04, y = 0.1, measured at −100 °C to 300 °C.

$x$$Bi_{0.5}K_{0.5}Zr_{0.9}Sn_{0.1}O_3$ ceramics with $0 \le x \le 0.02$.[15] The mixed phases can be easily found in the ceramics with $0.025 \le x \le 0.05$ with an increase in BKZS contents, while the specific phase compositions of each sample needs to be further confirmed by their corresponding ε_r–T curves (see Figure 2). As shown in Figure 2, both $T_{R\text{-}O}$ (≤−65 °C) and $T_{O\text{-}T}$ (≥86 °C) can be clearly observed in the composition range of 0–0.02 (see Figure 2a–c), further confirming our conclusion.[15,16] Furthermore, $T_{O\text{-}T}$ (~70 °C) of the ceramics with x = 0.025 is above room temperature, while $T_{R\text{-}O}$ (~−59 °C) is far below room temperature (see Figure 2d). Thus, we can deduce that the O-T phase boundary was formed in the ceramics with x = 0.025. One can see from Figure 2e,f that $T_{O\text{-}T}$ (62 °C → 59 °C) gradually shifts toward room temperature, and $T_{R\text{-}O}$ is gradually compressed and is near room temperature. Therefore, the R, O, and T phases should coexist in the ceramics with x = 0.03–0.035. Finally, there is only one obvious dielectric peak for the ceramics with $0.04 \le x \le 0.05$; that is, the R-T phase boundary can be driven by modifying x values, where $T_{R\text{-}T}$ is 33 °C, 18 °C, and 12 °C for x = 0.04, 0.045, and 0.05, respectively (see Figure 2g–i). As a result, the phase structure of $(1-x)(K_{0.4}Na_{0.6})(Nb_{0.96}Sb_{0.04})O_3$-$xBi_{0.5}K_{0.5}Zr_{0.9}Sn_{0.1}O_3$ ceramics is shown here: $0 \le x \le 0.02$ for an O phase, x = 0.025 for O-T mixed phases, $0.03 \le x \le 0.035$ for R-O-T, and $0.04 \le x \le 0.05$ for R-T. To further clarify the phase evolutions, we investigated the influences of Sn contents on the phase structure of the ceramics. However, there are different trends for the 0.96-$(K_{0.4}Na_{0.6})(Nb_{0.96}Sb_{0.04})O_3$-$0.04Bi_{0.5}K_{0.5}Zr_{1-y}Sn_yO_3$ ceramics, as shown in Figure 1b. By using a similar method, the R-T phase boundary and R single phase were observed in the ceramics with $0 \le y \le 0.4$ and $0.5 \le y \le 1.0$, respectively (see Figures 1b and 3).

To investigate the effects of x and y contents on the Curie temperature (T_C), we plotted the ε_r–T curves of the ceramics as a function of x and y, measured at 100 kHz and 30–450 °C, as shown in Figure 4a,c. Figure 4b,d addresses the phase diagrams of $(1-x)(K_{0.4}Na_{0.6})(Nb_{0.96}Sb_{0.04})O_3$-$xBi_{0.5}K_{0.5}Zr_{1-y}Sn_yO_3$ ceramics, which were established by the data derived from the ε_r–T curves (see Figures 2, 3, and 4a,d). One can find that BKZS and Sn contents have different effects on their phase transitions. As shown in Figure 4b,d, the T_C values linearly decreased with increasing BKZS contents, while T_C slowly decreased with increasing Sn contents, indicating that Zr can more quickly reduce T_C of KNN with respect to

DOI: 10.1021/acsami.5b00151
ACS Appl. Mater. Interfaces 2015, 7, 5927–5937

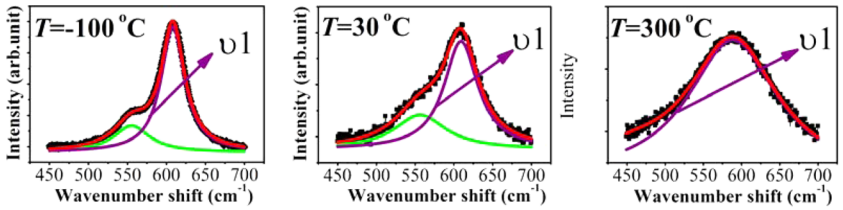

Figure 6. Magnified and fitted Raman spectra as a function of T = −100 °C, 30 °C, 300 °C in the wavenumber ranges from 450 to 700 cm^{-1} of the ceramics with x = 0.04, y = 0.1.

Sn.[3,4,9,15,16] In addition, we can see from Figure 4b that the BKZS can increase $T_{R\text{-}O}$ and decrease $T_{O\text{-}T}$ simultaneously, as Sb^{5+} does.[15,16] As a result, the O phase zone of the ceramics was compressed gradually with the increase of x. The R-O-T and R-T phase boundaries are formed in the ceramics with $0.03 \leq x \leq 0.035$ and $0.04 \leq x \leq 0.05$, respectively. In contrast, we can find from Figure 4d that the appropriate Sn content will induce the increase of $T_{R\text{-}T}$ gradually. In addition, one can see that the ε_r−T curves of the ceramics with $y \geq 0.5$ become flatter, and there are no obvious abnormal dielectric peaks in the temperature range of −100−400 °C, thus leading to the formation of R phase. In addition, we can also conjecture that the ceramics with $y \geq 0.5$ belong to be R phase according to the results of XRD and ferroelectricity.

It is well-known that some debates on the phase structure still exist for $BaTiO_3$-based ceramics.[25−29] For example, recent research has revealed that there is an intermediate orthorhombic phase of the R-T phase boundary in $BaTiO_3$-based ceramics.[27] Therefore, we suspected that an intermediate phase also exists in KNN-based ceramics of this work. To further understand the phase structure, we measured the temperature (−100 °C to 300 °C) dependence of the Raman spectrum of the ceramics with x = 0.04 and y = 0.1, as shown in Figure 5. What should be pointed out is that the measured Raman frequency range is from 50 to 1000 cm^{-1}. According to the literature,[28] we magnified the Raman spectrum in the wavenumber range of 450 to 700 cm^{-1} after background subtraction. In addition, the two peaks of the Raman spectrum are simulated by the Lorentzian method, which correspond to ν1 (~600 cm^{-1}) and ν2 (~550 cm^{-1}) modes, as shown in Figure 6. Figure 6 only shows the Raman spectrum of the ceramics as a function of T = −100 °C, 30 °C, and 300 °C, and other data are shown in Figure S1 of Supporting Information. One can see that the ν1 modes associated with the BO_6 perovskite octahedron shift with varied temperatures,[28,29] indicating that the temperatures induced the phase transition. Figure 7 shows the temperature dependence of the ν1 mode and dielectric permittivity of the ceramics with x = 0.04 and y = 0.1. More interestingly, there is only one Raman anomalous peak located at room temperature, which matches its corresponding ε_r−T curve. As a result, the O phase was completely compressed; that is, there is no intermediate phase of the R-T phase boundary in the ceramics with x = 0.04 and y = 0.1.

Figure 8a−h shows the FE-SEM surface images of the ceramics with different BKZS and Sn contents. In addition, we also counted the grain size distributions of the ceramics as a function of x and y, as shown in Figure 9. One can find that the grain sizes of the ceramics show a strongly compositional dependence. As shown in Figures 8a−d and 9a−d, the grain sizes of a pure KNNS ceramic distribute homogeneously, and a bimodal grain distribution was found in the compositions of x =

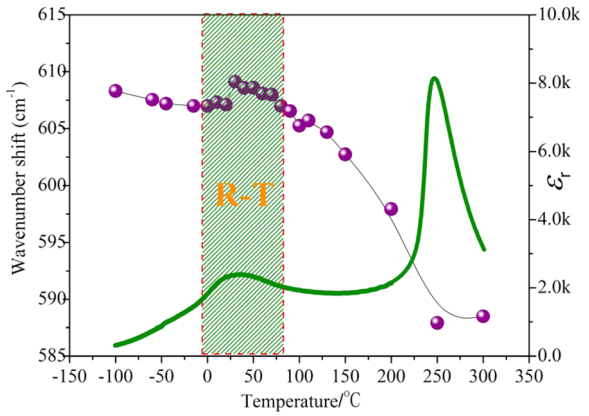

Figure 7. The evolution of the ν1 mode and dielectric permittivity results of the ceramics with x = 0.04, y = 0.1 as a function of temperature ranging from −100 °C to 300 °C.

0.02−0.05. In addition, the refined grains fill the gaps of large ones, resulting in the formation of dense microstructure, which is also important for the enhanced electrical properties.[15,16] A similar phenomenon was also found in the ceramics with y = 0 and 0.03, as shown in Figures 8e,f and 9e,f. More interestingly, one can see from Figures 8g,h and 9g,h that the ceramics with y = 0.6 and 1.0 possess very small grains, which is the reason why the ε_r−T curves were seriously compressed in the ceramics with $0.5 \leq y \leq 1.0$. To analyze the Sn element distribution, its element mapping of the ceramics with x = 0.04 and y = 0.1 was characterized using the energy-dispersive X-ray analysis, as shown in Figure 8i. One can see that a homogeneous Sn^{4+} distribution was shown in the ceramics with x = 0.04 and y = 0.1.

Figure 10a,c show the P−E loops of the ceramics as a function of x and y, measured at f = 10 Hz and room temperature. It can be seen that all ceramics have typical P−E loops, indicating that all compositions are ferroelectrics. To analyze the influences of BKZS and Sn contents on the ferroelectric properties of the ceramics, we plotted their remnant polarization (P_r) and the coercive field (E_C), as shown in Figure 10b,d. A higher P_r and a lower E_C were simultaneously observed in the phase boundary region ($0.025 \leq x \leq 0.05$), while a similar changing trend of P_r and E_C was observed in the ceramics with different Sn contents. It is worth noting that relatively high P_r values can be achieved in the phase boundary region ($0.025 \leq x \leq 0.05$ and $0 \leq y \leq 0.4$). In this work, the existence of different phase boundaries (e.g., O-T, R-O-T, and R-T) promotes the rotation of polarization vector.[15−18] At last, the ferroelectricity of the ceramics has been enhanced.

Figure 11a,b shows the room-temperature dielectric constant (ε_r) and dielectric loss (tan δ) of the ceramics as a function of x and y, measured at f = 100 kHz. One can see from Figure 11a

DOI: 10.1021/acsami.5b00151
ACS Appl. Mater. Interfaces 2015, 7, 5927−5937

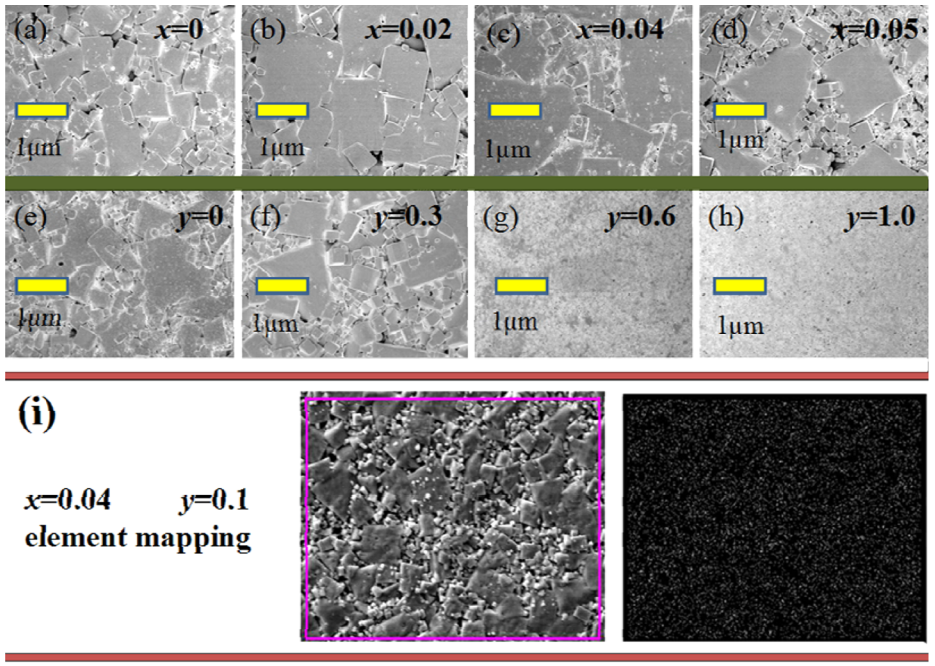

Figure 8. FE-SEMV surface images of the ceramics with (a–d) x = 0, 0.02, 0.04, 0.05. (e–h) y = 0, 0.3, 0.6, 1.0. (i) Sn element mapping of the surface in the ceramics with x = 0.04, y = 0.1.

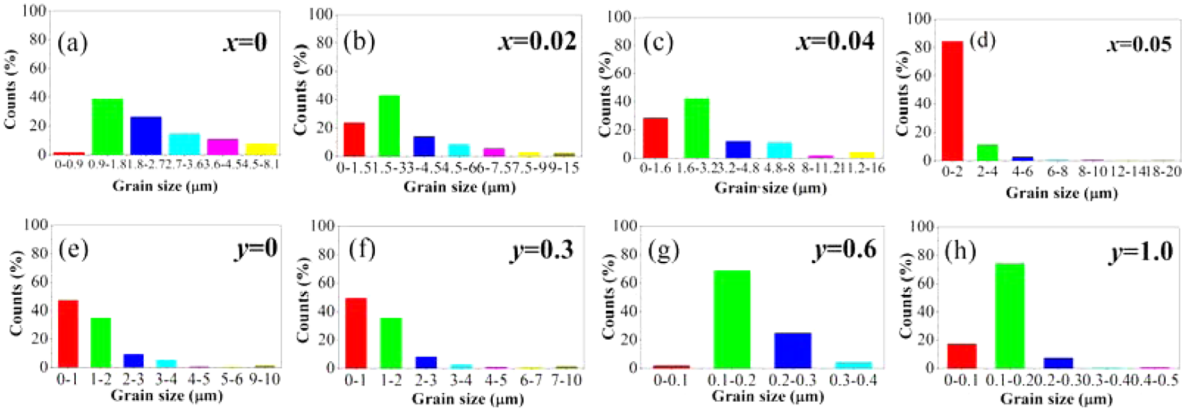

Figure 9. Grain size distribution of the surface morphologies of the ceramics with (a–d) x = 0, 0.02, 0.04, 0.05. (e–h) y = 0, 0.3, 0.6, 1.0.

that ε_r increases continuously with the addition of BKZS and then fluctuates for $0.03 \leq x \leq 0.05$. We can find from Figure 11b that ε_r keeps a higher value, fluctuates in the ceramics with $0 \leq y \leq 0.4$, and then decreases gradually with the further increase of y. In addition, the tan δ of the two diagrams exhibits a similar trend, almost keeping unchanged values (~0.04) with the compositions near the phase boundary region. As a result, the dielectric properties of the ceramics can also be enhanced due to the formation of the phase boundaries.[15−18]

Figure 12 shows the composition dependence of d_{33}, k_p, and $\varepsilon_r P_r$ in the ceramics. One can see that d_{33} increases first and then decreases with the increase of x and y, reaching a peak value of ~460 pC/N for x = 0.04 and y = 0.1. At the same time, we can notice that a large d_{33} (415−460 pC/N) is also obtained in the ceramics with R-O-T and R-T phase boundary regions ($0.03 \leq x \leq 0.045$), as shown in Figure 12a. With respect to other compositions near the R-T phase boundary ($0.04 \leq x \leq 0.045$), the ceramics with x = 0.05 possess a relatively lower d_{33} value (~360 pC/N) due to a lower $T_{R\text{-}T}$ (~12 °C).[19] However, the piezoelectric activity almost disappears for ceramics with a high Sn content ($0.5 \leq y \leq 1.0$) (see Figure 12b), which is consistent with other reported results.[4] As known to all, the existence of phase boundaries is one important reason for enhanced d_{33}.[15−17] Furthermore, the equation of $d_{33} \sim \varepsilon_r P_r$ can also be used to illuminate the physical mechanisms of the improved d_{33}.[15,16] Therefore, we plotted the curves of $\varepsilon_r P_r$ against x and y, as shown in Figure 12c,d. One can see that both $\varepsilon_r P_r$ and d_{33} can exhibit a similar changing trend, getting a relatively high value in the phase boundary region. As a result, enhanced d_{33} also partly comes from the improvement of both ε_r and P_r.[15,16]

In the past, some authors investigated the strain of KNN-based ceramics,[11−14] and some interesting results have been attained. Recently, F. Rubio-Marcos et al. have developed KNN-based microfiber ceramics with a high strain of 0.17% under a low driving electric field of 3 kV/mm.[40] Figure 13a,c plots the bipolar strain curves of the ceramics as a function of x and y, measured at f = 10 Hz and room temperature. Typical butterfly shape strain curves can be found in the ceramics. In addition, each sample exhibits obvious hysteresis effect and

DOI: 10.1021/acsami.5b00151
ACS Appl. Mater. Interfaces 2015, 7, 5927−5937

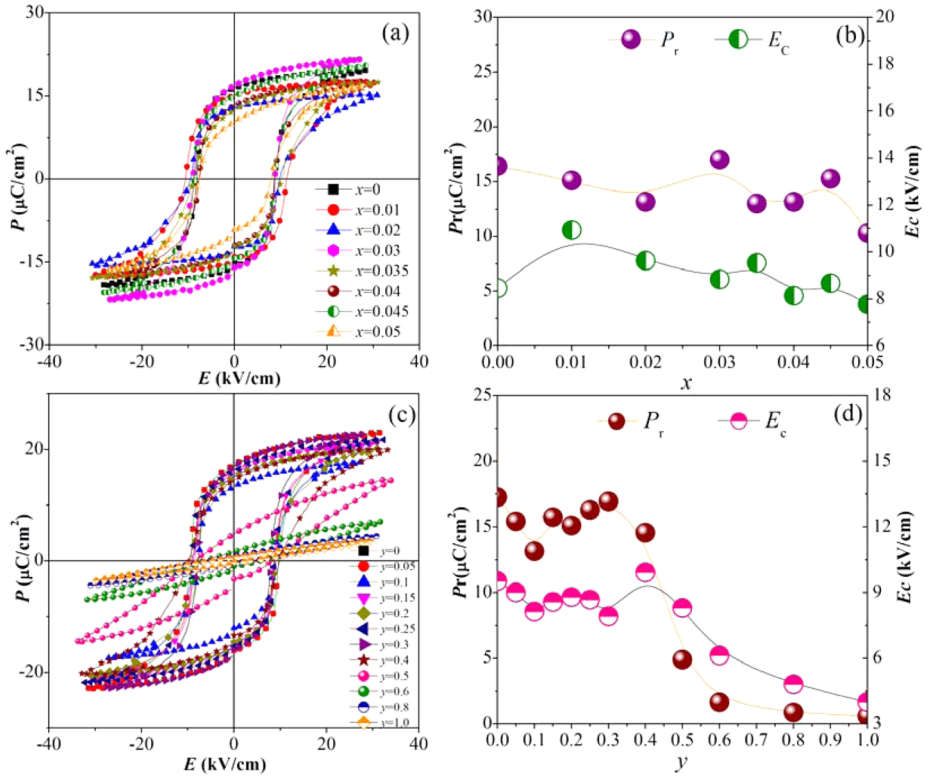

Figure 10. (a and c) P–E loops of the ceramics as a function of x and y content. (b and d) P_r and E_C against x and y content, respectively.

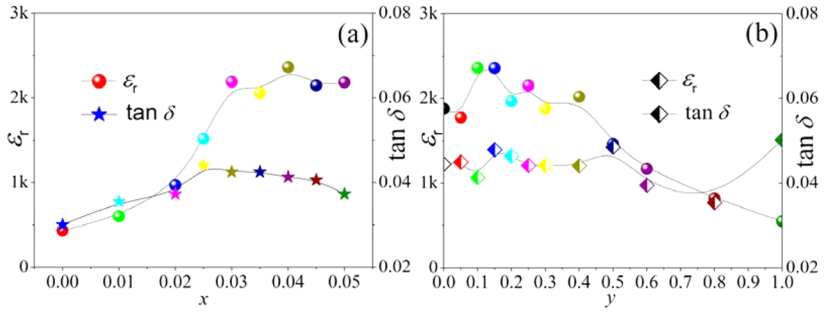

Figure 11. (a and b) ε_r and tan δ of the ceramics as a function of x and y content, respectively.

relatively small negative strain. Figure 13b,d shows the composition dependence of strain and d_{33}* of the ceramics. One can see that both strain and d_{33}* present a similar changing trend. As shown in Figure 13b, a high d_{33}* of 869–880 pm/V was attained in the R-O-T phase boundary region ($0.03 \leq x \leq 0.035$), which is higher with respect to other compositions being close O-T ($x = 0.025$) or R-T phase boundary ($0.04 \leq x \leq 0.05$). That is to say, both a high d_{33}* of 880 pm/V and a strain of 0.22% under a low driving electric field of 3 kV/mm can be achieved in ceramics with $x = 0.03$ and $y = 0.1$ due to the existence of multiphase regions (e.g., R-O-T phase boundary).[6,12] Furthermore, we can find from Figure 13d that the d_{33}* increases gradually with the increase of y, reaching a maximum value of 875 pm/V for $x = 0.04$ and $y = 0.4$. The results indicate that the strain of the ceramics will be affected by its phase boundary as well as Sn content.

Generally speaking, a strong d_{33} (~460 pC/N) can be achieved in the ceramics with R-T phase boundary ($x = 0.04$, $y = 0.1$), and a large d_{33}* (~880 pm/V) can be attained in the ceramics with R-O-T phase boundary ($x = 0.03$, $y = 0.1$). Subsequently, we discussed the correlations and differences between d_{33} and d_{33}* and explored the relationships between piezoelectricity and phase boundary. First, there is an obvious difference between d_{33}* and d_{33}. The d_{33}* of each sample is superior to their corresponding d_{33}, because their testing method is different and moreover the non-180° domain wall motions may extrinsically ascribe to the strain response.[12] Second, there is the same origin of piezoelectricity (d_{33}) and strain property (d_{33}*), which originates from the phase boundary and domain switching.[15−17,20−23] Third, as mentioned above, largest d_{33} (~460 pC/N) and d_{33}* (~880 pm/V) in this work were observed in the ceramics with $x = 0.04$, $y = 0.1$, and $x = 0.03$, $y = 0.1$, respectively. It is usually accepted that the R-T phase boundary mainly contributes to the improved d_{33},[15−17] and the multiphase coexistence plays an important role in the enhanced d_{33}*.[6,12] Therefore, d_{33} of this work was promoted in the R-T phase boundary region, while d_{33}* was enhanced in the R-O-T phase boundary region. In addition, one can find that d_{33}* increases gradually with the increase of Sn content, reaching a large d_{33}* (~875 pm/V) for the ceramics with $x = 0.04$ and $y = 0.4$. The results indicate that the Sn content plays an important role in the enhanced strain of

DOI: 10.1021/acsami.5b00151
ACS Appl. Mater. Interfaces 2015, 7, 5927−5937

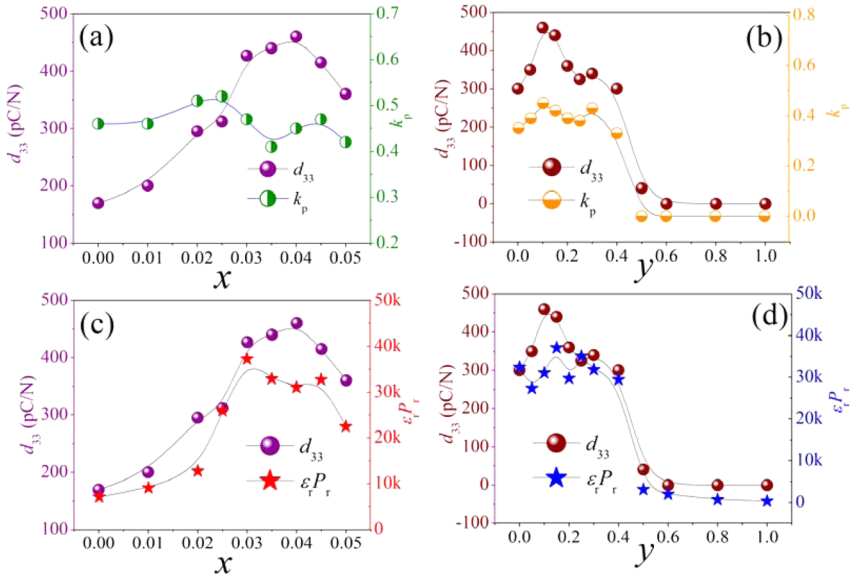

Figure 12. d_{33}, k_p of the ceramics as a function of (a) x and (b) y content. d_{33} and $\varepsilon_r P_r$ of the ceramics as a function of (c) x and (d) y content.

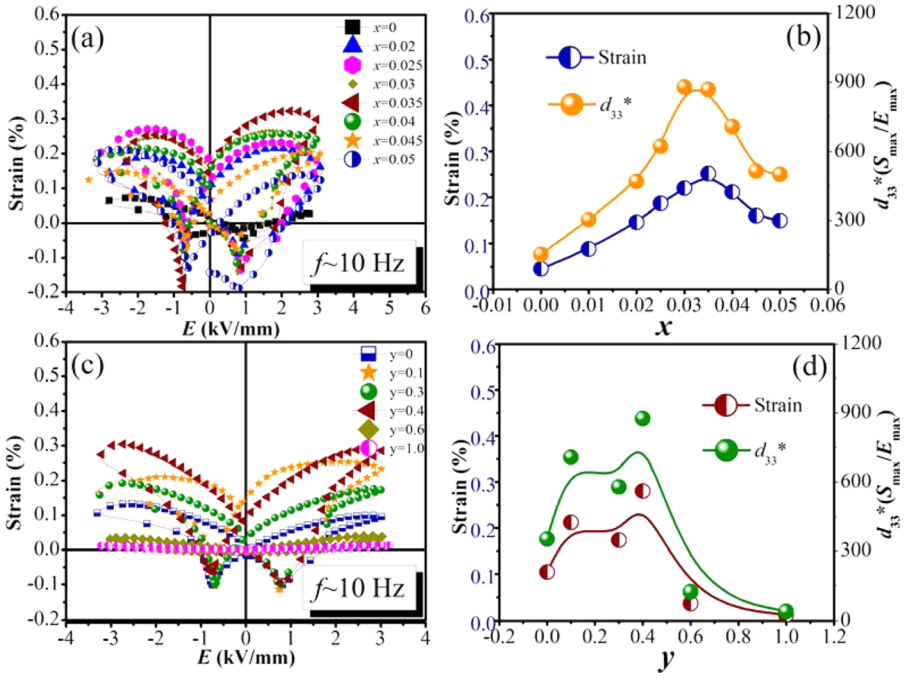

Figure 13. Electric field-induced strain curves of the ceramics as a function of (a) x content and (c) y content. Strain and d_{33}* of the ceramics as a function of (b) x content and (d) y content.

this work, and thus the KNN material system containing Sn^{4+} was a useful way to promote their strain properties. That is to say, d_{33} and strain in KNN ceramics are decided by not only phase boundary but also the compositions. As a result, excellent comprehensive electrical properties ($d_{33} \sim 427$ pC/N, d_{33}* $\sim$ 880 pm/V, $k_p \sim 47\%$, $T_C \sim 268$ °C) were observed in the ceramics with $x = 0.03$ and $y = 0.1$, which are superior to other reported results in KNN-based ceramics (see Table 1).

Figure 14a–d shows the composition dependence of thermal stability of d_{33}. There is a strong composition dependence of thermal stability of d_{33}. As shown in Figure 14a, d_{33} of the ceramics with $x = 0$ keeps an almost unchanged value with the increase of annealing temperatures (T_a), which is in agreement with the previous reports.[24] For the ceramics with $x > 0$, d_{33} decreases slowly and then drops sharply when T_a is near T_C. Figure 14b shows d_{33} vs x measured at room temperature and $T_a \sim T_C$. One can see that a high d_{33} of >300 pC/N can be observed for $0.03 \leq x \leq 0.045$ even if T_a almost approaches T_C. That is, even if the ceramics exhibit a slightly poor thermal stability of d_{33}, a larger d_{33} can effectively solve this issue. In addition, the addition of optimum Sn content ($y \leq 0.2$) can promote the thermal stability of d_{33} (see Figure 14c,d), while their stability decreases gradually with further increasing y.

CONCLUSION

In this work, our objective is to promote both piezoelectric properties and strain of the KNN-based ceramics by constructing multiphase coexistence and then identify the

DOI: 10.1021/acsami.5b00151
ACS Appl. Mater. Interfaces 2015, 7, 5927–5937

Table 1. Relationship between Phase Boundary and Piezoelectricity in Piezoceramics

material system	compositions	phase boundary	d_{33} pC/N	strain %	d_{33}* pm/V	T_C (°C)	ref
Pb-based	PZT4	R-T	410	-	700	250	30
Bi-layered	$(Na_{0.78}K_{0.22})_{0.5}TiO_3$-$xBi(Mg_{0.5}Ti_{0.5})O_3$	T	-	0.35	636	~270	32
$BaTiO_3$ -based	$BaTiO_3-(0.4CaTiO_3-0.6BaSnO_3)$	R-O-T	570	0.07	1444	~70	33
BNT-based	$0.94(1-x)Bi_{0.5}Na_{0.5}TiO_3-0.06BaTiO_3-xK_{0.5}Na_{0.5}NbO_3$	-	<100	0.45	560	-	2
KNN-based	$(K_{0.44}Na_{0.52}Li_{0.04})(Nb_{0.84}Ta_{0.10}Sb_{0.06})O_3$	O-T	416	-	750	253	10
	$K_{0.5-x/2}Na_{0.5-x/2}Li_{ix}NbO_3$	O-T	240	-	220	460	11
	$K_{0.5-x/2}Na_{0.5-x/2}Li_xNb_{1-y}Ta_yO_3$	O-T	190	-	310	310	11
	$0.92(Na_{0.535}K_{0.48})NbO_3-0.08LiNbO_3$	O-T	324	0.054	538	-	12
	$(K_{1-x}Na_x)_{0.92}Li_{0.08}NbO_3$	R-O-T	110	0.18	450	~480	13
	$K_{0.5}Na_{0.5}Nb_{0.7}Ta_{0.3}O_3$	-	-	0.11	270	~200	34
	$(Na_{0.52}K_{0.48})(Nb_{1-x}Sb_x)O_3$ $x = 0.12$	-	230	0.32	800	-	35
	$(1-x)(K_{0.4}Na_{0.6})(Nb_{0.96}Sb_{0.04})O_3$-$xBi_{0.5}K_{0.5}Zr_{1-y}Sn_yO_3$ ($x = 0.03$, $y = 0.1$)	R-O-T	427	0.22	880	~268	this work
	$(1-x)(K_{0.4}Na_{0.6})(Nb_{0.96}Sb_{0.04})O_3$-$xBi_{0.5}K_{0.5}Zr_{1-y}Sn_yO_3$ ($x = 0.04$, $y = 0.1$)	R-T	460	0.212	707	246	this work

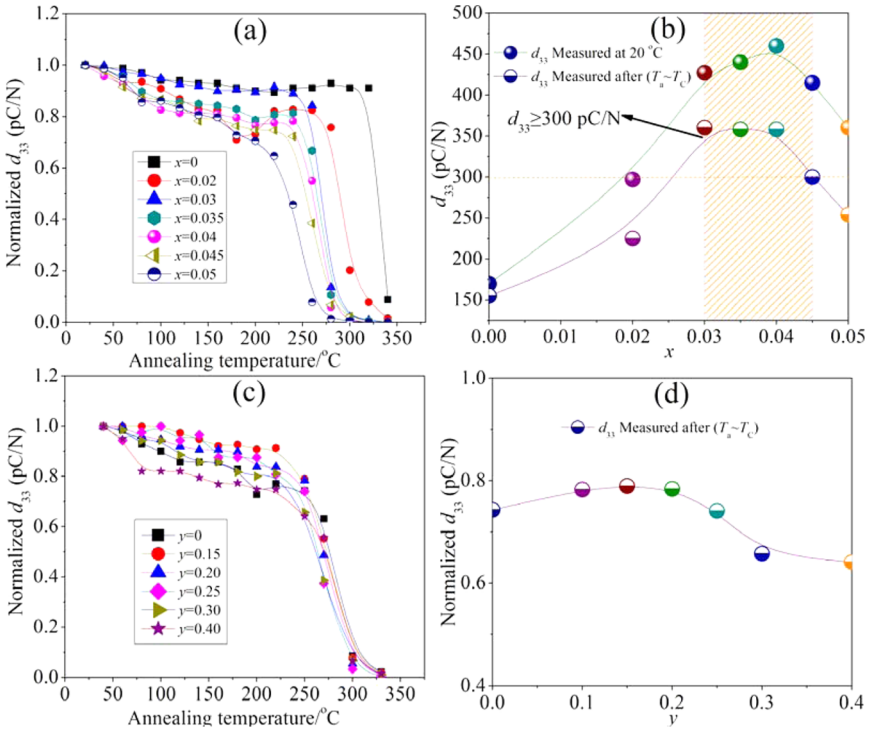

Figure 14. (a and c) d_{33} vs annealing temperature of the ceramics with different x and y, (b) d_{33} of the ceramics with different x contents measured at room temperature and $T_a \sim T_C$, and (d) normalized d_{33} of the ceramics with different y contents measured at $T_a \sim T_C$.

corresponding phase compositions. By our efforts, we developed a high strain and a large d_{33} in $(1-x)(K_{0.4}Na_{0.6})$-$(Nb_{0.96}Sb_{0.04})O_3$-$xBi_{0.5}K_{0.5}Zr_{1-y}Sn_yO_3$ ceramics by constructing new phase boundaries using the addition of BNKZ as well as Sn^{4+}. The R-T phase boundary can be well confirmed by the temperature dependence of the dielectric constant and Raman spectrum as well as XRD patterns. The ceramic system possesses a large d_{33}* ~ 880 pm/V and a high d_{33} ~ 460 pC/N by refining their compositions. The formation of R-O-T and R-T phase boundaries as well as the doping of Sn^{4+} are largely responsible for the improvement of d_{33}* and d_{33}. As a result, we believe that this material system can benefit the further development of potassium−sodium niobate ceramics.

■ ASSOCIATED CONTENT

Supporting Information

Magnified and fitted Raman spectra in wavenumber ranges from 450 to 700 cm^{-1} of the ceramics. This material is available free of charge via the Internet at http://pubs.acs.org.

■ AUTHOR INFORMATION

Corresponding Author

*E-mail: msewujg@scu.edu.cn; wujiagang0208@163.com.

Notes

The authors declare no competing financial interest.

■ ACKNOWLEDGMENTS

Authors gratefully acknowledge support from the National Science Foundation of China (NSFC nos. 51102173,

DOI: 10.1021/acsami.5b00151
ACS Appl. Mater. Interfaces 2015, 7, 5927−5937

51272164, 51332003, and 51472169), the Fundamental Research Funds for the Central Universities (2012SCU04A01), and the College of Materials Science and Engineering of Sichuan University. Ms. Hui Wang is thanked for measuring the SEM images.

REFERENCES

(1) Jaffe, B.; Cook, W. R.; Jaffe, H. *Piezoelectric Ceramics*; Academic: New York, 1971.
(2) Zhang, S. T.; Kounga, A. B.; Aulbach, E.; Ehrenberg, H.; Rödel, J. Giant Strain in Lead-Free Piezoceramics $Bi_{0.5}Na_{0.5}TiO_3$−$BaTiO_3$−$K_{0.5}Na_{0.5}NbO_3$ System. *Appl. Phys. Lett.* **2007**, *91*, 112906.
(3) Hyoung, S. H.; Wook, J.; Kang, J. K.; Chang, W. A.; Kim, W. I.; Kyoung, K. A.; Jae, S. L. Incipient Piezoelectrics and Electrostriction Behavior in Sn-Doped $Bi_{1/2}(Na_{0.82}K_{0.18})_{1/2}TiO_3$ Lead-Free Ceramics. *J. Appl. Phys.* **2013**, *113*, 154102.
(4) Lee, J. S.; Pham, K. N.; Han, H. S.; Lee, H. B.; Tran, V. D. N. Strain Enhancement of Lead-Free $Bi_{1/2}(Na_{0.82}K_{0.18})_{1/2}TiO_3$ Ceramics by Sn Doping. *J. Korean Phys. Soc.* **2012**, *60* (2), 212−215.
(5) Xue, D.; Zhou, Y.; Bao, H.; Gao, J.; Zhou, C.; Ren, X. Large Piezoelectric Effect in Pb-Free $Ba(Ti,Sn)O_3$-$x(Ba,Ca)TiO_3$ Ceramics. *Appl. Phys. Lett.* **2011**, *99*, 122901.
(6) Zhou, P.; Zhang, B.; Zhao, L.; Zhao, X.; Zhu, L.; Cheng, L.; Li, J. High Piezoelectricity Due to Multiphase Coexistence in Low-Temperature Sintered $(Ba,Ca)(Ti,Sn)O_3$−$CuOx$ Ceramics. *Appl. Phys. Lett.* **2013**, *103*, 172904.
(7) Li, W.; Xu, Z.; Chu, R.; Zeng, H.; Zhao, K. Enlarged Polymorphic Phase Transition Boundary and Enhanced Piezoelectricity in Ternary Component $0.8Ba_{1-x}Ca_xTiO_3$−$0.1BaTi_{0.8}Zr_{0.2}O_3$−$0.1BaTi_{0.9}Sn_{0.1}O_3$ Ceramics. *Mater. Lett.* **2013**, *110*, 80−82.
(8) Brahem, R.; Rahmouni, H.; Farhat, N.; Dhahri, J.; Khirouni, K.; Costa, L. C. Electrical Properties of Sn-Doped $Ba_{0.75}Sr_{0.25}Ti_{0.95}O_3$ Perovskite. *Ceram. Int.* **2014**, *40*, 9355−9360.
(9) Veselinovic, L.; Mitric, M.; Mancic, L.; Vukomanovic, M.; Hadzic, B.; Markovic, S.; Uskokovic, D. The Effect of Sn for Ti Substitution on the Average and Local Crystal Structure of $BaTi_{1-x}Sn_xO_3$ ($0 \le x \le 0.20$). *J. Appl. Crystallogr.* **2014**, *47*, 999−1007.
(10) Saito, Y.; Takao, H.; Tani, T.; Nonoyama, T.; Takatori, K.; Homma, T.; Nagaya, T.; Nakamura, M. Lead-Free Piezoceramics. *Nature* **2004**, *432*, 84−87.
(11) Hollenstein, E.; Davis, M.; Damjanovic, D.; Setter, N. Piezoelectric Properties of Li- and Ta-Modified $(K_{0.5}Na_{0.5})NbO_3$ Ceramics. *Appl. Phys. Lett.* **2005**, *87*, 182905.
(12) Wang, K.; Li, J. F.; Zhou, J. J. High Normalized Strain Obtained in Li-Modified $(K,Na)NbO_3$ Lead-Free Piezoceramics. *Appl. Phys. Express* **2011**, *4*, 061501.
(13) Yan, K.; Ren, X. B. Multi-phase Transition Behaviour and Large Electrostrain in Lead-Free $(K, Na, Li)NbO_3$ Ceramics. *J. Phys. D: Appl. Phys.* **2014**, *47*, 015309.
(14) Matsubara, M.; Yamaguchi, T.; Kikuta, K.; Hirano, S. Effect of Li Substitution on the Piezoelectric Properties of Potassium Sodium Niobate Ceramics. *Jpn. J. Appl. Phys.* **2005**, *44*, 6136−6142.
(15) Wang, X. P.; Wu, J. G.; Xiao, D. Q.; Zhu, J. G.; Cheng, X. J.; Zheng, T.; Zhang, B. Y.; Lou, X. J.; Wang, X. J. Giant Piezoelectricity in Potassium−Sodium Niobate Lead-Free Ceramics. *J. Am. Chem. Soc.* **2014**, *136* (7), 2905−2910.
(16) Zheng, T.; Wu, J. G.; Cheng, X. J.; Wang, X. P.; Zhang, B. Y.; Xiao, D. Q.; Zhu, J. G.; Lou, X. J. New Potassium−Sodium Niobate Material System: A Giant-d_{33} and High-T_C Lead-Free Piezoelectric. *Dalton Trans.* **2014**, *43* (30), 11759−11766.
(17) Zuo, R. Z.; Fu, J. Rhombohedral−Tetragonal Phase Coexistence and Piezoelectric Properties of $(NaK)(NbSb)O_3$−$LiTaO_3$−$BaZrO_3$ Lead-Free Ceramics. *J. Am. Ceram. Soc.* **2011**, *94*, 1467−1470.
(18) Cheng, X. J.; Wu, J. G.; Wang, X. P.; Zhang, B. Y.; Zhu, J. G.; Xiao, D. Q. New Lead-Free Piezoelectric Ceramics Based on $(K_{0.48}Na_{0.52})(Nb_{0.95}Ta_{0.05})O_3$−$Bi_{0.5}(Na_{0.7}K_{0.2}Li_{0.1})_{0.5}ZrO_3$. *Dalton Trans.* **2014**, *43*, 9419.
(19) Liang, W. F.; Wu, W. J.; Xiao, D. Q.; Zhu, J. G. Effect of the Addition of $CaZrO_3$ and $LiNbO_3$ on the Phase Transitions and Piezoelectric Properties of $K_{0.5}Na_{0.5}NbO_3$ Lead-Free Ceramics. *J. Am. Ceram. Soc.* **2011**, *94* (12), 4317−4322.
(20) Fu, J.; Zuo, R. Giant Electrostrains Accompanying the Evolution of a Relaxor Behavior in $Bi(Mg,Ti)O_3$−$PbZrO_3$ −$PbTiO_3$ Ferroelectric Ceramics. *Acta Mater.* **2013**, *61*, 3687−3694.
(21) Cross, L. E. Ferroelectric Materials for Electromechanical Transducer Applications. *Mater. Chem. Phys.* **1996**, *43*, 108.
(22) Ren, X. Large Electric-Field-Induced Strain in Ferroelectric Crystals by Point-Defect-Mediated Reversible Domain Switching. *Nat. Mater.* **2004**, *3*, 91−94.
(23) Xu, Y. H.; Hong, W.; Feng, Y. J.; Tan, X. L. Antiferroelectricity Induced by Electric Field in $NaNbO_3$-Based Lead-Free Ceramics. *Appl. Phys. Lett.* **2014**, *104*, 052903.
(24) Gao, Y.; Zhang, J. L.; Zong, X. J.; Wang, C. L.; Li, J. C. Extremely Temperature-Stable Piezoelectric Properties of Orthorhombic Phase in $(K,Na)NbO_3$-Based Ceramics. *J. Appl. Phys.* **2010**, *107*, 074101.
(25) Keeble, D. S.; Benabdallah, F.; Thomas, P. A.; Maglione, M.; Kreise, J. Revised Structural Phase Diagram of $(Ba_{0.7}Ca_{0.3}TiO_3)$-$(BaZr_{0.2}Ti_{0.8}O_3)$. *Appl. Phys. Lett.* **2013**, *102* (9), 092903.
(26) Lummen, T. T.; Gu, Y.; Wang, J.; Lei, S.; Xue, F.; Kumar, A.; Barnes, A. T.; Barnes, E.; Denev, S.; Belianinov, A. Thermotropic Phase Boundaries in Classic Ferroelectrics. *Nat. Commun.* **2014**, *5*, 3172−3180.
(27) Zhang, L.; Zhang, M.; Wang, L.; Zhou, C.; Zhang, Z.; Yao, Y.; Zhang, L.; Xue, D.; Lou, X.; Ren, X. Phase Transitions and the Piezoelectricity Around Morphotropic Phase Boundary in $Ba(Zr_{0.2}Ti_{0.8})O_3$-$x(Ba_{0.7}Ca_{0.3})TiO_3$ Lead-Free Solid Solution. *Appl. Phys. Lett.* **2014**, *105*, 162908.
(28) Kakimoto, K.; Akao, K.; Guo, Y.; Ohsato, H. Raman Scattering Study of Piezoelectric $(Na_{0.5}K_{0.5})NbO_3$-$LiNbO_3$ Ceramics. *Jpn. J. Appl. Phys.* **2005**, *44*, 7064.
(29) Klein, N.; Hollenstein, E.; Damjanovic, D.; Trodahl, H. J.; Setter, N.; Kuball, M. A Study of the Phase Diagram of $(K,Na,Li)NbO_3$ Determined by Dielectric and Piezoelectric Measurements, and Raman Spectroscopy. *J. Appl. Phys.* **2007**, *102*, 014112.
(30) Saito, Y. Hysteresis Curve of X-ray Diffraction Peak Intensity in Lead Zirconate Titanate Ceramics. *Jpn. J. Appl. Phys.* **1997**, *36*, 5963−5969.
(31) Zeb, A.; Milne, S. J. Large Electromechanical Strain in Lead-Free Binary System $K_{0.5}Bi_{0.5}TiO_3$-$Bi(Mg_{0.5}Ti_{0.5})O_3$. *J. Am. Ceram. Soc.* **2014**, 2413−2415.
(32) Aman, U.; Chang, W. A.; Amir, U.; Ill, W. K. Large Strain Under a Low Electric Field in Lead-Free Bismuth-Based Piezoelectrics. *Appl. Phys. Lett.* **2013**, *103*, 022906.
(33) Zhu, L. F.; Zhang, B. P.; Zhao, L.; Li, J. F. High Piezoelectricity of $BaTiO_3$−$CaTiO_3$−$BaSnO_3$ Lead-Free Ceramics. *J. Mater. Chem. C* **2014**, *2*, 4764−4771.
(34) Matsubara, M.; Kikuta, K.; Hirano, S. Piezoelectric Properties of $(K_{0.5}Na_{0.5})(Nb_{1-x}Ta_x)O_3$−$K_{5.4}CuTa_{10}O_{29}$ Ceramics. *J. Appl. Phys.* **2005**, *97*, 114105.
(35) Fu, J.; Zuo, R. Z.; Qi, H.; Zhang, C.; Li, J. F.; Li, L. T. Low Electric-Field Driven Ultrahigh Electrostrains in Sb-Substituted $(Na,K)NbO_3$ Lead-Free Ferroelectric Ceramics. *Appl. Phys. Lett.* **2014**, *105*, 242903.
(36) Rubio-Marcos, F.; Ochoa, P.; Fernandez, J. F. Sintering and Properties of Lead-Free $(K,Na,Li)(Nb,Ta,Sb)O_3$ Ceramics. *J. Eur. Ceram. Soc.* **2007**, *27* (13), 4125−4129.
(37) Rubio-Marcos, F.; Del Campo, A.; López-Juárez, R.; Romero, J. J.; Fernández, J. F. High Spatial Resolution Structure of $(K,Na)NbO_3$ Lead-Free Ferroelectric Domains. *J. Mater. Chem.* **2012**, *22* (19), 9714−9720.
(38) Rubio-Marcos, F.; Marchet, P.; Romero, J. J.; Fernández, J. F. Structural, Microstructural and Electrical Properties Evolution of $(K,Na,Li)(Nb,Ta,Sb)O_3$ Lead-Free Piezoceramics Through NiO Doping. *J. Eur. Ceram. Soc.* **2011**, *31* (13), 2309−2317.

DOI: 10.1021/acsami.5b00151
ACS Appl. Mater. Interfaces 2015, 7, 5927−5937

(39) Rubio-Marcosa, F.; Romero, J. J.; Martin-Gonzalez, M. S.; Fernández, J. F. Effect of Stoichiometry and Milling Processes in the Synthesis and the Piezoelectric Properties of Modified KNN Nanoparticles by Solid State Reaction. *J. Eur. Ceram. Soc.* **2010**, *30* (13), 2763−2771.
(40) Bortolani, F.; Del Campo, A.; Fernandez, J. F.; Clemens, F.; Rubio-Marcos, F. High Strain in $(K,Na)NbO_3$-Based Lead-Free Piezoelectric Fibers. *Chem. Mater.* **2014**, *26*, 3838−3848.

DOI: 10.1021/acsami.5b00151
ACS Appl. Mater. Interfaces 2015, 7, 5927−5937